Journal of Materials Science: Materials in Electronics (2018) 29:13810–13817
https://doi.org/10.1007/s10854-018-9512-3

Strong red emission and enhanced electrostrain in $(Bi_{0.5}Na_{0.5})_{0.935-x}Pr_xBa_{0.065}Ti_{1-x}Sb_xO_3$ lead-free multifunctional ceramics

Cen Liang[1] · Jigong Hao[1] · Wei Li[1] · Juan Du[1] · Peng Fu[1] · Zhijun Xu[2] · Ruiqing Chu[2] · Zhicheng Guan[3]

Received: 19 April 2018 / Accepted: 16 June 2018 / Published online: 25 June 2018

Abstract
Lead-free perovskite $(Bi_{0.5}Na_{0.5})_{0.935-x}Pr_xBa_{0.065}Ti_{1-x}Sb_xO_3$ (BNBT6.5–*x*PS) ceramics are prepared by ordinary sintering technique. The compositional dependence of phase structure, electrical and photoluminescence properties of the ceramics was systematically investigated. Results showed that all samples exhibit pure perovskite structure with dense microstructures. With the addition of PS, a strong red emission located at 610 nm and a weak red emission at 660 nm under a light 450 nm excitation was observed. The strong red emission band is ascribed to the inter-4f transition from the excited $^1D_2$ to the ground state $^3H_4$ and the weak red emission located at 660 nm is due to the $^3P_0 \rightarrow {}^3F_2$ transition. And then the BNBT6.5–0.004PS ceramic exhibited the strongest photoluminescence property. Besides the excellent photoluminescence properties, PS modifications induced an enhanced filed-induced strain. At $x = 0.001$, a large strain of 0.31% was obtained at a driving field of 70 kV/cm. As a multifunctional material, it has potential application as a multifunctional device such as optical-electro integration and coupling device applications.

1 Introduction

Piezoelectric ceramics are a kind of functional ceramics with wide application. They are widely used in sensors, brakes, converters and other equipment. Since the last half century, lead zirconate titanate (PZT) ceramics had a great used in application field [1]. However, the PZT is toxicity because of its large amount of lead oxide [2]. And the high vapor pressure is needed in preparation of PZT ceramics [2]. Therefore, to protect the environmental, people have to develop the lead-free ceramics, and after more than 20 years hard work people have been made a great progress. Nowadays, lead-free piezoelectric ceramics are considered perfect substitute for materials in piezoelectric industry [3–5], so new and lead-free piezoelectric ceramics become one of the hot materials in some countries for the sake of environmental friendly development and sustainable development of human society. Unfortunately, many of the lead-free piezoelectric ceramics are not as good as lead-based ones [6]. In order to get better properties of lead-free ceramics, people are trying to find out new materials and methods [3].

The $Bi_{0.5}Na_{0.5}TiO_3$ (BNT)-based lead-free ceramics are provided with intriguing structural and piezoelectric properties [7]. BNT is a relatively strong ferroelectric body. At room temperature (RT), it has a considerable residual polarization strength (P_r = 38 μC/cm^2) and larger coercivity (E_c = 73 kV/cm). At present, the excellent performance of BNT base ceramics has been widely concerned by scholars all over the world, and it is considered that BNT is one promising lead-free ceramics to replace lead based piezoelectric ceramics [2]. However, the pure BNT ceramics are unsatisfactory in the piezoelectric properties [8]. The doping of other materials in BNT is used to enhance its piezoelectric properties. So a new BNT-based solid solution is obtained, such as BNT–$BaTiO_3$ (BNT–BT) binary system [8]. The morphotropic phase boundary (MPB) mainly exists between the rhombohedral and tetragonal perovskite phases. Ceramics samples show

✉ Jigong Hao
haojigong@lcu.edu.cn

✉ Wei Li
liwei@lcu.edu.cn

1 College of Materials Science and Engineering, Liaocheng University, Liaocheng 252059, People's Republic of China

2 School of Environmental and Materials Engineering, Yantai University, Yantai 264005, People's Republic of China

3 North United Power Co., Ltd. Dalate Power Plant, Hohhot, China

promising piezoelectric properties in MPB, and MPB is found in the BNT-based of x = 0.006–0.007 [9–12].Nevertheless, at the composition with the highest piezoelectric properties, the minimum value for the depolarization temperature T_d is always found. Obviously, low T_d values are undesirable in fabricating high-performance BNT-based ceramics, since temperature stability of properties is one of the most important issues for many applications.

On the other hand, having a low T_d is very important for achieving a large electric-field strain. A giant electric-field-induced strain appeared when the T_d is decreased to room temperature. There are two aspects to consider if you want to get a large strain in BNT-based ceramics [13, 14]: one is the base composition, the large polarization strain should be inherent in these components, eg in BNT–BT–KNN system, MPB compositions of BNT–BT [15, 16]; the other aspect is the chemical modifications, some chemical elements may be destroy the long-range ferroelectric order of ceramic materials and make it disorder, then this ferroelectric disorder become orderly again because of electric field is applied [13, 17, 18]. BNT–BT or BNT–BKT solid solution dope some chemical entities such as metal dopants [17–22] or $ABO_3/A_2B_2O_6$-type compounds [13–16, 23–26], it can be observed in these materials near the MPB have good performance, therefore the optimal strain performance of BNT-based ceramics can be improved by chemical doping.

In recent years, multifunctional materials have led to extensive scientific research, such materials often have two or more properties. For example, in ferroelectric materials introduced with trivalent REs elements [27], a new multifunctional luminescence property was found because rare elements are thought to be the luminescent centers of luminescent materials [28, 29]. Furthermore, the electrical properties can be improve in piezoelectric materials by using rare earth (RE) elements to break ferroelectric order [30]. For the BNT-based materials with high-strain, RE has a strong disruption action on the long-range ferroelectric order of BNT-based materials, so it has been proved to be a good modifier to enhance the strain performance of BNT-based ceramics. Then, due to its luminescent characteristic, multifunctional BNT-based materials with excellent luminescence and high-strain properties are easily fabricated.

Recently, our research groups have reported electric field-induced giant strain response and excellent photoluminescence-enhancement effect in RE^{3+}-modified BNT-based ceramics [24, 31, 32], confirming the role of the RE^{3+}. Following our previous work, in the present work, lead-free perovskite $(Bi_{0.5}Na_{0.5})_{0.935-x}Pr_xBa_{0.065}Ti_{1-x}Sb_xO_3$ (BNBT6.5–*x*PS) ceramics are fabricated and the phase structure, electrical and photoluminescence properties of the ceramics was studied on the basis of different composition.

2 Experimental

$(Bi_{0.5}Na_{0.5})_{0.935-x}Pr_xBa_{0.065}Ti_{1-x}Sb_xO_3$ (BNBT6.5–*x*PS) lead-free ceramic was prepared by conventional ceramic fabrication technique: solid-state reaction technique. The $BaCO_3$ (99%), Na_2CO_3 (99.8%), TiO_2 (99.5%), Bi_2O_3 (99.9%), Pr_6O_{11} (99.9%) and Sb_2O_3 (99%) form Sinopharm Chemical Reagent were as starting materials. The first step of the experiment was to dry the raw materials and weigh them. Then ball-milled for 12 h, and when the ball-milled, it was important to add some alcohol to the ball pots. The ball ground powders were dried and mixed powers were put into a calcined of alumina crucible at 850 °C for 4 h. After the calcinations, starting second ball-milled for 12 h. Polyvinyl alcohol (PVA) was added to the powers for granulation and the powers were pressed into pieces using a certain mould. After burning off the PVA at 550 °C for 5 h, the dish samples were sintered at 1120 °C for 2 h.

The ceramic-related Phase structure were identified by X-ray diffraction (XRD, Bruker D8 Advance, Germany) with Cu Ka radiation. A field-emission scanning electron microscope (FE-SEM, Carl Zeiss, merlin compact) was used to identify the surface morphology of ceramic. In the experiment, we tend to be on both sides of the ceramic coated with sliver paste, respectively, the formation of the electrode was the ceramic chip calcined under 850 °C for 10 min. A broad frequency dielectric spectrometer (Concept 80, Novocontrol Inc, Germany) research the temperature dependences of the ceramic dielectric properties. To test the depolarization temperature (T_d), firstly the ceramic was polarized by applying a high voltage, then ceramic in use of aix-ACCT TF2000FE-HV ferroelectric unit (aix-ACCT Inc, Germany) to determine the T_d by measuring the thermally stimulated depolarization currents (TSDC). The electric-field-induced polarization (*P*–*E*) and strain (*S*–*E*) measurements were disclosed by an aix-ACCTTF2000FE-HV ferroelectric test unit (aix-ACCT Inc, Germany) connected with an accessory laser interferometer vibrometer (SP-S120/500; SIOS Mebtechnik GmbH, Germany). The spectrofluorometer (FLS920, Edinburgh Instruments, UK) was primarily used to test photoluminescence excitation (PLE) and photoluminescence (PL) spectra.

3 Result and discussion

Figure 1 shows XRD patterns of BNBT6.5–*x*PS ($x = 0 \sim 0.004$) ceramics sintered at 1120 °C. From the patterns, there was no impurity peaks appear and a single perovskite-type solid solution structure in all samples, indicating that the rare earth element Pr and element

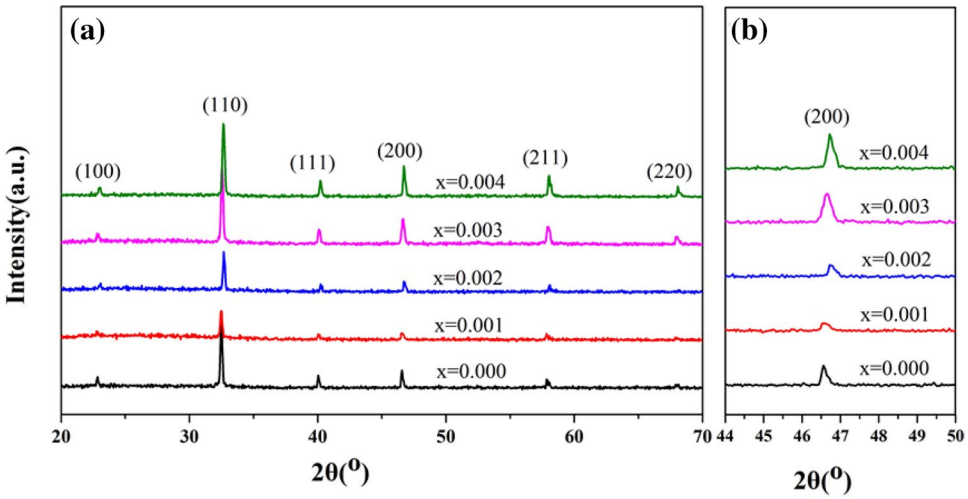

Fig. 1 XRD patterns of BNBT6.5–*x*PS samples in the 2θ range of 20°–70°

Sb have been fully incorporated into the matrix to form homogeneous blends. This can be further confirmed by the shift of characteristic diffraction peaks as shown in the Fig. 1b. In the present work, smaller Pr^{3+} (1.126 Å) would enter A site of the BNBT6.5, replacing Na^{+} (1.39 Å) and Bi^{3+} (1.30 Å) the location of the site. Simultaneously, in BNBT–*x*PS ceramics the larger Sb^{3+} (0.76 Å) replaced the smaller Ti^{4+} (0.605 Å). According to the relevant report BNT ceramics at room temperature was oblique square hexahedral phase with single (200) diffraction peak near 46.5° [2]. In the studied BNBT6.5–*x*PS system, peak of (200) was not split, suggesting the BNBT6.5–*x*PS ceramics had a similar phase structure to that of pure BNT without regard to PS concentration.

Figure 2 gives the micrographs of BNBT6.5–*x*PS ($x = 0.001 \sim 0.004$) ceramics observed on the surface of the composition, it can be seen from the picture that the crystal cells were developed and had dense microstructure. When the content of PS was different, the microstructure had no significant change in the picture, so the the microstructure of the ceramics was hardly affected by PS content.

The hysteresis loops measured at 10 Hz and RT are shown in Fig. 3a. In this picture, we can see that pure BNBT6.5 ceramics had typical ferroelectric behavior and shown good saturation hysteresis loop. As can be seen from the picture, as the PS content increases, the shape of the hysteresis loops begin to shrink. Thus it can be explained that the long-term ferroelectric sequence was modified by PS. With

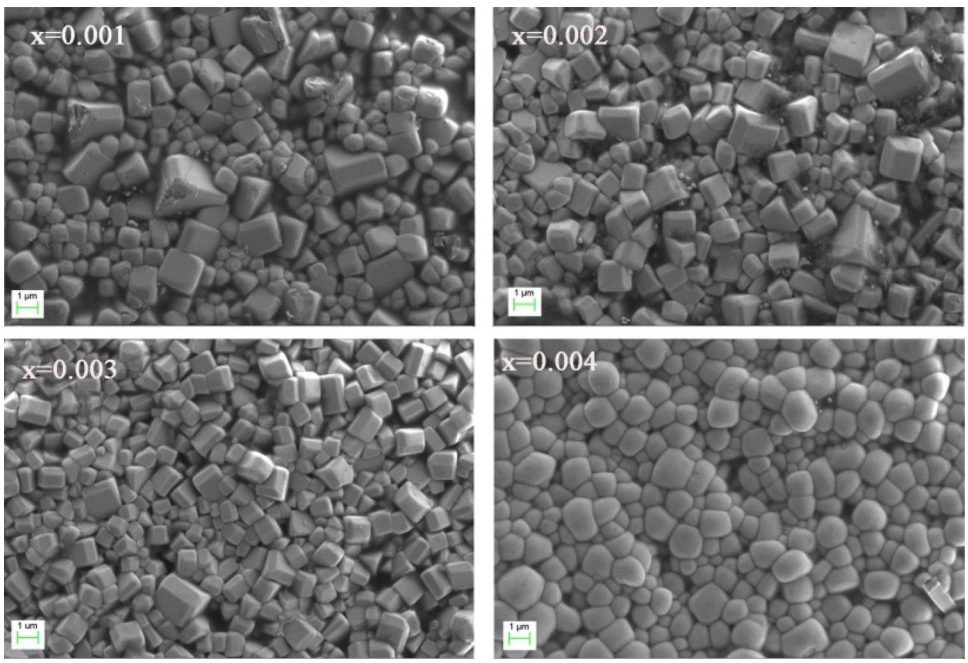

Fig. 2 SEM images of BNBT6.5–*x*PS ceramics with $x = 0.001$, 0.002, 0.003, 0.004

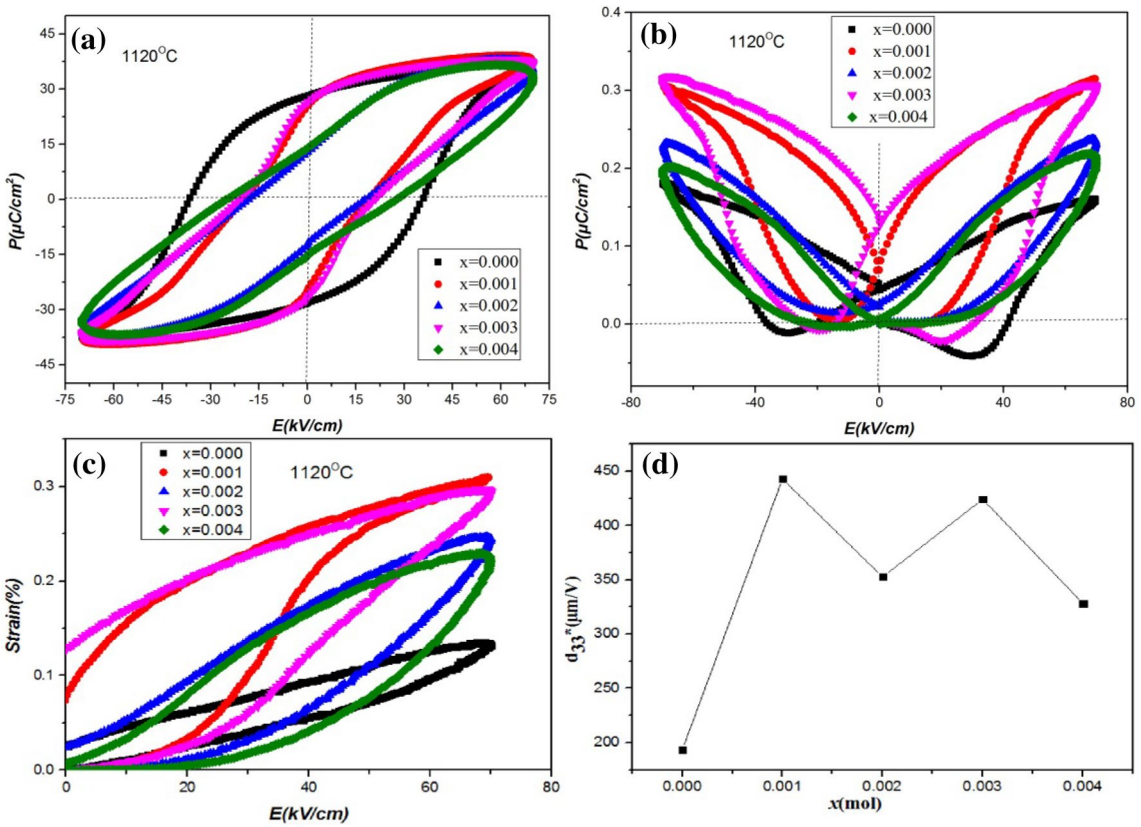

Fig. 3 **a** *P–E* hysteresis loops, **b** bipolar strain curves, **c** unipolar strain curves and **d** the large signal d_{33}^{*} of BNBT6.5–*x*PS measured at RT and 10 Hz

the interference of ferroelectric order, the *P–E* loops with "pinched" appeared at $x = 0.001$, it indicated that there was ergodic relaxation under zero electric-field [33]. Figure 3b shows bipolar strain curves of BNBT6.5–*x*PS ceramics recorded at 10 Hz and RT. The butterfly strain hysteresis loop and the visible negative strain S_{neg} of pure BNBT6.5 were typical ferroelectric behaviors, both of which related to the bipolar cycles, the reason was that the domain back was switched during the cycle [34]. With the addition of PS, when the doping amount was 0.001, the butterfly like loop changed and became the shape of the sprout, meanwhile, S_{neg} gradually increased until it disappeared to zero, and when S_{neg} begin disappeared, there would be an increase of positive strain S_{pos}, and in Fig. 3c a significant increase of unipolar strain. This confirmed the appearances of the ergodic relaxor phase. At $x = 0.001$, the value of unipolar strain S_{uni} measured up a maximum is 0.31%, 442.93 pm/V was corresponding large signal d_{33}^{*} (S_{max}/E_{max}).

The dielectric constant (ε_r) and dielectric loss ($\tan\delta$) versus the temperature of the BNBT6.5–*x*PS ($x = 0.000 \sim 0.004$) piezoelectric ceramics at 1 MHz are shown in Fig. 4a. From Fig. 4a, there were two dielectric anomalies in two-phase transitions in pure BNBT6.5 samples and it was to made known in the temperature properties of the dependent loss tangent. The dielectric anomaly at high temperature, denoted by the temperature of maximum ε_r, was consider to be contact with a slack of tetragonal polar nano-regions(PNRs) emerged from rhombohedral PNRs [35]. At lower temperature, the dielectric anomaly was now believed to be aroused through thermal evolutions of discrete PNRs [35]. While it was previously we thought it was due to the transformation of "anti-ferroelectric" state, achieved the depolarization temperature T_d. Recently, T_d was measured by testing polarized sampled, using the thermally stimulated depolarization currents (TSDC) [36]. Regarding polarized BNBT6.5–*x*PS samples, Fig. 4b shows the j_{TSDC} dependence of temperature. It wasobserved that the T_d moved to RT as PS content increases, proving the ferroelectric relaxation phase change was caused by the change of components [37].

The impedance spectra of the BNBT6.5–*x*PS ceramics with $x = 0.001$, 0.002, 0.003, 0.004 in the frequency limit from 0.01 Hz to 20 MHz over 500–700 °C are shown in Fig. 5a–d. There was one Debye-like semicircle in BNBT6.5–*x*PS ceramics, which indicated that in the measured temperature range for all samples the impedance was controlled by a single localized relaxation mechanism [25]. Furthermore, the total conductivities of the ceramics were obtained by analyzing complex impedance data, Fig. 5e

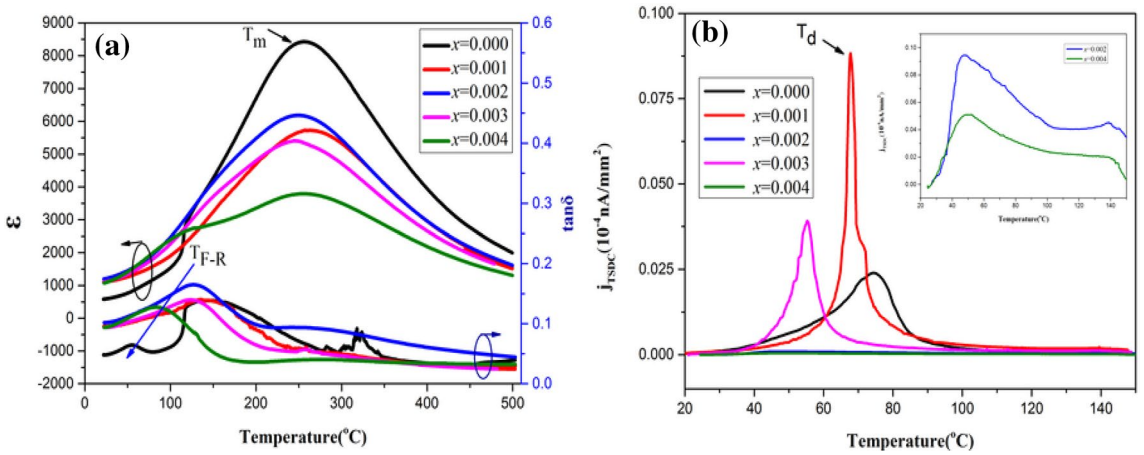

Fig. 4 **a** The dielectric constant (ε_r) and dielectric loss (tanδ) versus the temperature of BNBT6.5–*x*PS ($x=0.000$,0.001, 0.002, 0.003, 0.004) ceramics at 1 MHz. **b** The thermoelectric current of ceramics change with temperature

shows the logarithms of conductivity (σ) versus mutual temperature 1000/T of the BNBT6.5–*x*PS ceramics. The activation energy (E_a) was calculated according to the Arrhenius relationship: $\rho=\rho_o\cdot\exp(E_a/k_BT)$, where k_B is Boltzmann constant, ρ_o is the pre-exponential factor, E_a is activation energy and T is absolute temperature [38, 39]. The corresponding activation energies E_a for BNBT6.5–*x*PS, was 1.05, 1.06, 0.82 and 1.21 eV, for $x=0.001$, 0.002, 0.003, and 0.004, respectively. This result indicated that the movement of oxygen vacancies was responsible for DC conduction process [40]. As reported that, in ABO_3 perovskite materials, the E_a value of A-site cation was 4, and 12 eV was the E_a value of B-site cation [41]. In terms of oxygen vacancy, the E_a value was uncertain, but it also varied from 0.5 to 2 eV, the E_a value changed with the concentration of different oxygen vacancy [42]. Therefore, it can draw a conclusion that in 500 to 700 °C temperature range oxygen vacancies dominate. Additionally, the improvement of E_a by Pr^{3+} and Sb^{3+} ions modification can be resulted in the oxygen vacancies decreasing.

Figure 6a shows the photoluminescence excitation (PLE) ($\lambda_{em}=610$ nm) and photoluminescence (PL) ($\lambda_{ex}=450$ nm) spectra of BNBT6.5–*x*PS at RT. Both the excitation and emission peaks did not change for all the BNBT6.5–*x*PS ceramics. When the emission wavelength of 610 nm was fixed, the excitation spectrum was observed, there was a excitation peak near 440 nm, as well as a excitation peak located 475 nm and a excitation peak near 490 nm. There was also a wide excitation band between 350 and 450 nm, which may be due to the charged transformation from Pr^{3+} (4f) → Ti (3d) and the absorption of Bi^{3+} ions [43, 44]. Meanwhile, the peak near 450 nm corresponded to the $^3H_4 \rightarrow {}^3P_2$ transition, the peak at 475 nm was $^3H_4 \rightarrow {}^3P_1$ transition, and the $^3H_4 \rightarrow {}^3P_0$ transition corresponded to the peak near 490 nm. The ^3P_J (J = 0, 1, 2) transition from $^3H_4$ was a typical 4f-4f transition, which was the reason for this result [29, 45]. The PL spectrum shown two red emission bands under the 450 nm excitation: the peak near 610 nm was a strong red emission peak and the peak near 660 nm was a weak red emission. The inter-4f transition from $^1D_2$ to $^3H_4$ was the cause of the strong red emission band [46, 47]. The transition from $^3P_0$ to $^3F_2$ was thought to be responsible for weak red emission at 660 nm [48, 49]. As show in Fig. 6b of the energy level diagram for Pr^{3+}, the red line was the transformation from $^1D_2$ to $^3H_4$ and the orange line was about the transition of $^3P_0 \rightarrow {}^3F_2$.

Figure 7a shows the strength of red emission near 610 nm of BNBT6.5–*x*PS ceramics under a light 450 nm excitation. The results shown that the emission peak intensity tend to reduce when x from 0.001 to 0.002. And then, as the content of PS increased, BNBT6.5–*x*PS ceramics also shown stronger and stronger emission intensity, reaching the maximum when $x=0.004$, it was suggest that the luminescent intensity increases with the number of the luminescent centers. Furthermore, the emission spectrum of the BNBT6.5–0.004PS ceramic was used to determine the CIE chromaticity coordinates. As shown in Fig. 7b, $x=0.6651$, $y=0.3346$ were positioned as CIE chromaticity coordinates, from which the red color is produced when Pr^{3+} doped into BNBT6.5–*x*PS ceramics.

4 Conclusion

In this work, BNBT6.5–*x*PS ceramics were prepared by solid-phase sintering, so that the ceramics had field-induced large strain and shown bright red emission. They were a king of multifunctional ferroelectric ceramics. The results showed that the ceramics of pure BNBT6.5 doped PS induced the phase change, which was the

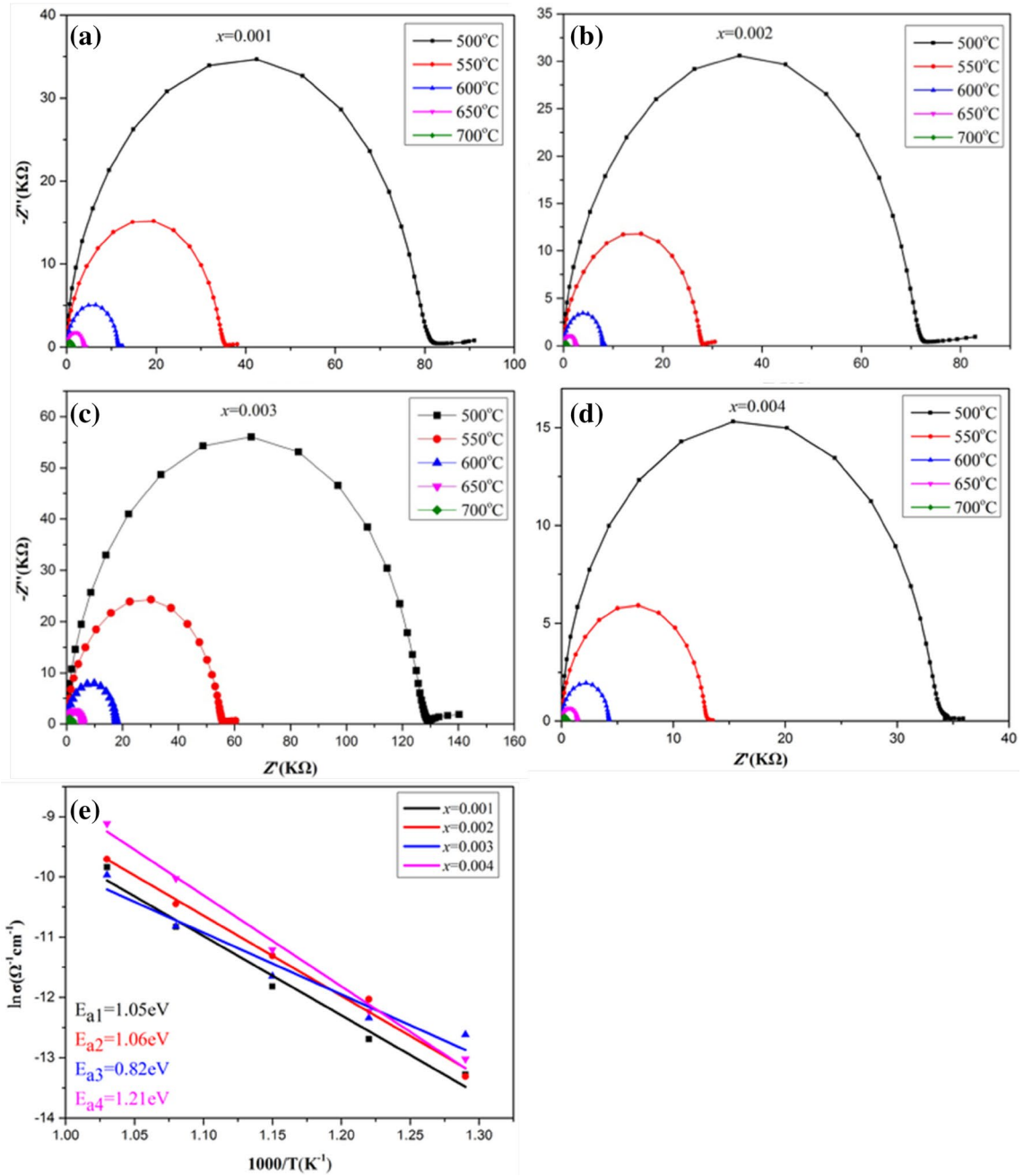

Fig. 5 The impedance spectra of the BNBT6.5–*x*PS ceramics, **a** $x=0.001$; **b** $x=0.002$; **c** $x=0.003$ and **d** $x=0.004$ ceramics in the frequency range of 0.01 Hz to 20 MHz over 500–700 °C and **e** Arrhenius plots of σdc conductivity of the BNBT6.5–*x*PS ceramics

transformation from ferroelectric phase to ergodic relaxor phase. At $x=0.001$, the value of unipolar strain S_{uni} reached a maximum value of 0.31% and received a large signal d^*_{33} (S_{max}/E_{max}) of 407 pm/V. Upon 450 nm excitation, two distinct emission bands were observed: a strong red light emission is found at 610 nm and a weak red emission at 660 nm. Strong emission bands corresponded to the transition from $^1D_2$ to $^3H_4$ and weak emission bands was $^3P_0 \rightarrow {}^3F_2$ transition. The samples with $x=0.004$ shown the optimal photoluminescence. The samples from this experiment can be used as multifunctional materials because of their excellent properties and the hope of expanding application through luminescent and piezoelectric properties.

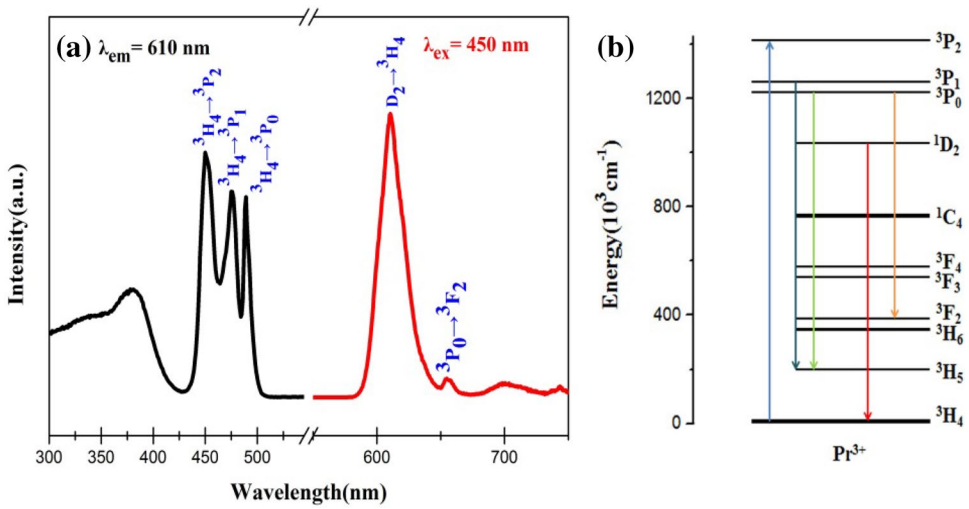

Fig. 6 **a** Room temperature PL (λ_{ex} = 450 nm) and PLE (λ_{em} = 610 nm) spectra of BNBT6.5–*x*PS. **b** The energy level diagram of Pr^{3+} ions

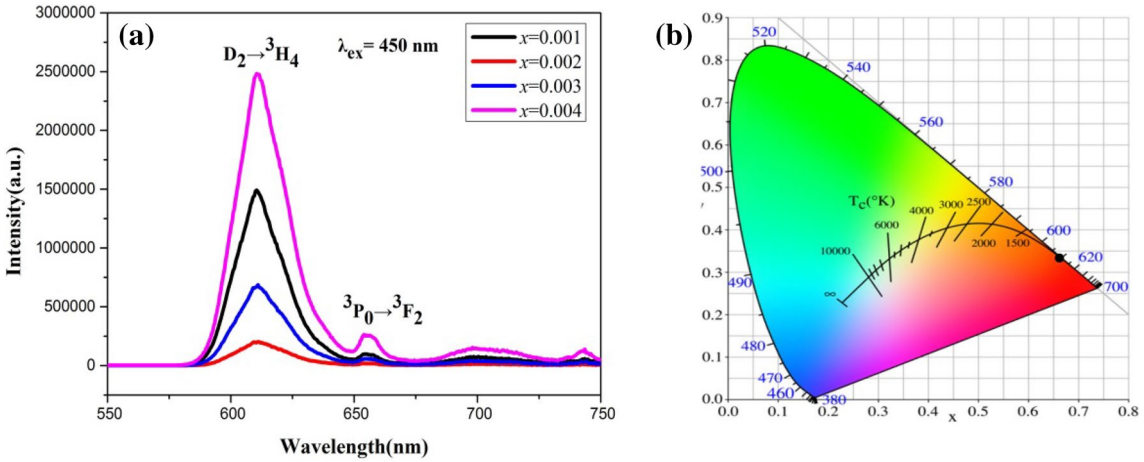

Fig. 7 **a** The PL spectra intensity dependence of Pr^{3+} ions concentrations excited at 450 nm, and **b** the calculated CIE chromaticity coordinates of BNBT6.5–0.004PS sample

Acknowledgements This work was supported by the National Key R&D Program of China (No. 2016YFB0402701); Focus on research and development plan in shandong province (No. 2017GGX202008); National Natural Science Foundation of China (Nos. 51402144 and 51502127); the Natural Science Foundation of Shandong Province of China (ZR2016EMM02).

References

1. B. Jaffe, W.R. Cook, H. Jaffe, *Piezoelectric Ceramics*, (Academic Press, London, 1971)
2. N. Chen, W. Yao, C. Liang, S. Xiao, J. Hao, Z. Xu, R. Chu, Ceram. Int. **42**, 9660–9666 (2016)
3. A. Hussain, J.U. Rahman, F. Ahmed, J.S. Kim, M.H. Kim, T.K. Song, W.J. Kim, J. Eur. Ceram. Soc. **35**, 919–925 (2015)
4. Y. Saito, H. Takao., T. Tani, T. Nonoyama, K. Takatori, T. Homma, M. Nakamura, Nature. **432**, 84 (2004)
5. J. Rödel, W. Jo, K.T. Seifert, E.M. Anton, T. Granzow, D. Damjanovic, J. Am. Ceram. Soc. **92**, 1153–1177 (2009)
6. S. Zhang, R. Xia, T.R. Shrout, J. Electroceram. **19**, 251–257 (2007)
7. W. Jo, R. Dittmer, M. Acosta, J. Zang, C. Groh, E. Sapper, J. Rödel, J. Electroceram. **29**, 71–93 (2012)
8. T. Takenaka, K.I. Maruyama, K. Sakata, J. Appl. Phys. **30**, 2236 (1991)
9. X. Liu, X. Xu, H. Du, J. Inorg. Mater. **33**, 683–687 (2018)
10. L. Li, J. Hao, Z. Xu, W. Li, R. Chu, Mater. Lett. **184**, 152–156 (2016)
11. X. Liu, J. Shi, F. Zhu, H. Du, T. Li, J. Inorg. Mater. 1–6 (2018)
12. W. Bai, P. Zheng, J. Wen, F. Zhang, D. Chen, J. Zhai, Z. Ji, Dalton. Trans. **46**, 15340–15353 (2017)
13. K. Wang, A. Hussain, W. Jo, J. Rödel, J. Am. Ceram. **95**, 2241–2247 (2012)
14. W. Bai, J. Xi, J. Zang, B. Shen, J. Zhai, H. Yan, J. Eur. Ceram. Soc. **35**, 2489–2499 (2015)
15. S.T. Zhang, A.B. Kounga, E. Aulbach, H. Ehrenberg, J. Rödel, Appl. Phys. Lett. **91**, 112906 (2007)

16. J. Hao, B. Shen, J. Zhai, C. Liu, X. Li, X. Gao, J. Appl. Phys. **113**, 114106 (2013)
17. J. Hao, Z. Xu, R. Chu, W. Li, P. Fu, J. Du, G. Li, J. Eur. Ceram. Soc. **36**, 4003–4014 (2016)
18. W. Bai, D. Chen, P. Zeng, B. Shen, J. Zhai, Z. Ji, Dalton. Trans. **45**, 8573–8586(2016)
19. X. Jia, J. Zang, Y. Gao, J. Wang, P. Zheng, Mater. Res. Bull. **89**, 11–15 (2017)
20. H.S. Han, W. Jo, J.K. Kang, J. Appl. Phys. **113**, 113–126 (2013)
21. B. Hu, Z. Pan, M. Dai, J. Am. Ceram. Soc. **97**, 3877–3882 (2015)
22. A. Hussain, C.W. Ahn, J.S. Lee, Sens. Actuators A. **158**, 84–89 (2010)
23. W. Bai, D. Chen, P. Zheng, J. Alloys Compd. **709**, 646–657 (2017)
24. Y. Chang, X. Sun, W. Xiong, J. Eur. Ceram. Soc. **37**, 859–864 (2017)
25. J. Hao, Z. Xu, R. Chu, J. Alloys Compd. **64**, 7857–7865 (2015)
26. W. Bai, D. Chen, P. Zheng, J. Xi, Y. Zhou, B. Shen, Z. Ji, J. Eur. Ceram. Soc. **37**, 2591–2604 (2017)
27. J. Hao, Z. Xu, R. Chu, S. Chu, W. Li, P. Fu, C. Hu, Mater. Lett. **193**, 138–141 (2017)
28. K. Ruan, X. Chen, T. Liang, J. Appl. Phys. **103**, 627 (2008)
29. H. Sun, D. Peng, X. Wang, J. Appl. Phys. **110**, 2087 (2011)
30. H. Sun, D. Peng, X. Wang, J. Appl. Phys. **111**, 2087 (2012)
31. J. Hao, Z. Xu, R. Chu, J. Eur. Ceram. Soc. **37**, 877–882 (2017)
32. J. Hao, Z. Xu, R. Chu, Scr. Mater. **122**, 10–13 (2016)
33. J. Hao, W. Bai, W. Li, J. Appl. Phys. **114**, 113 (2013)
34. K.T.P. Seifert, W. Jo, J. Rödel, J. Am. Ceram. **93**, 1392–1396 (2010)
35. J. Hao, X. Zhang, Z. Xu, Ceram. Int. **42**, 12964–12970 (2016)
36. E.M. Anton, W. Jo, D. Damjanovic, J. Appl. Phys. **110**, 094108 (2011)
37. L. Li, J. Hao, R. Chu, Dielectric. Ceram. Int. **42**, 9419–9425 (2016)
38. P. Fang, P. Liu, Z. Xi, J. Appl. Phys. **595**, 148–152 (2014)
39. Z. Peng, Y. Chen, Q. Chen J. Alloys Compd. **590**, 210–214 (2014)
40. S.S.N. Bharadwaja, S.B. Krupanidhi, J. Appl. Phys. **86**, 5862–5869 (1999)
41. B.S. Kang, S.K. Choi, C.H. Park, J. Appl. Phys. **94**, 1904–1911 (2003)
42. S. Steinsvik, R. Bugge, J. Gjønnes, J. Phys. Chem. Solids. **58**, 969–976 (1997)
43. J.L. Sommerdijk, A. Bril, A.W.D. Jager, J. Lumin. **8**, 341–343 (1974)
44. H. Zhou, G. Wu, F. Gao, IEEE Trans. Ultrason. Ferroelectr. Freq. Control. **57**, (2010)
45. L.S. Chi, R.S. Liu, B.J. Lee, J. Electrochem. Soc. **152**, J93–J98 (2005)
46. P.T. Diallo, K. Jeanlouis, P. Boutinaud J. Alloys Compd. **323**, 218–222 (2001)
47. R. Chen, D. Chen, J. Alloys Compd. **476**, 671–674 (2009)
48. D. Peng, H. Sung, X. Wang, J. Alloys Compd. **511**, 159–162 (2012)
49. Q.J. Chen, W.J. Zhang, X.Y. Huang, G.P. Dong, M.Y. Peng, Q.Y. Zhang, J. Alloys Compd. **513**, 139–144 (2012)